Performance of Shorted Microstrip Patch Antennas for Mobile Communications Handsets at 1800 MHz

Jack T. Rowley, *Member, IEEE*, and Rod B. Waterhouse, *Member, IEEE*

***Abstract*—We have investigated the application of two different types of novel shorted-patch antennas for mobile communications handsets at 1800 MHz. A single shorted-patch and a stacked shorted-patch antenna offering improved bandwidth are compared with data for a $\lambda/4$ monopole. The finite-difference time-domain (FDTD) technique was used to calculate antenna characteristics such as impedance and radiation patterns for two cases: on a handset and on a handset near a (2.5-mm voxel) heterogeneous head model in an actual position of phone use. We also obtained specific absorption rate (SAR) distributions and calculated the spatial peak 1-g SAR values. In addition, the effect on SAR and antenna characteristics of including a block model of the hand was assessed. Similar performance is achieved from the single or stacked shorted-patch antenna with the latter providing greater bandwidth, 8.2% versus 9.4% with the head and hand included. Both antennas reduce the 1-g spatial peak SAR value in the head by 70% relative to the monopole. The presence of the hand reduces the efficiency of all three antenna types by approximately 10%.**

***Index Terms*— Land-mobile radio, patch antennas, telephone sets.**

I. Introduction

THE increasing use of radio-based portable communications devices has created public concern about their safety despite reports finding no substantive scientific evidence of a long-term public health hazard [1], [2]. The proximity of these devices to the body during their operation leads to highly nonuniform exposure and so it is inappropriate to specify limits based on electric and magnetic fields or power density [3], [4]. Limits are therefore specified in terms of the actual rate of radio frequency energy absorption (specific absorption rate or SAR) with an averaging mass of 1 g [5] or 10 g [1] of tissue in the shape of a cube. Government agencies have announced plans to regulate portable radio transmitting devices based on these limits and this has led to a need for effective means of demonstrating compliance either through direct measurement of SAR or through electromagnetic (EM) computational methods [6]. Presently direct measurement methods are preferred due to the ability to quantify the accuracy of the system and the difficulties of modeling the intricate details of individual handsets [7].

The finite-difference time-domain (FDTD) technique has been used for a number of studies of the performance of antennas on mobile communications-type handsets [8]–[11]. We used a commercial code, XFDTD, purchased from Remcom Inc.[1] in our investigation [12]. The handset and $\lambda/4$ monopole dimensions used in this study are those specified in the canonical models of the European framework for Cooperation in Science and Technology Project COST244 [13]. These models were developed for comparison of results from different EM computational approaches and provided a useful starting point for the present study.

A 2.5-mm voxel resolution FDTD mesh of a male head and shoulders was used to analyze the performance of the antennas and the relative SAR's. This was based on a mesh obtained from Remcom Inc. and uses data from the Visible Human Project [14]. The dielectric properties assigned to the tissues at 1800 MHz were derived from the work of Gabriel [15], while the tissue mass densities were those supplied with the mesh [12]. The model was rotated to the intended position of use specified in the CENELEC draft standard on evaluation of SAR for mobile telecommunications equipment (MTE) [16]. This allows the perfect electrical conductor (PEC) edges of the handset to align with the FDTD grid and, thus, minimize staircasing errors. The presented antenna patterns were "corrected" for the rotation.

Present generation mobile telecommunications systems primarily operate in the 800–1000 MHz band with future systems being designed to operate in the 1.6–2 GHz band [6]. The move to the higher frequency band may allow the introduction of more sophisticated antenna types for handset applications. A number of authors have examined directional antennas for current generation handsets [17], [18], but the relatively large area required for these antennas has limited their commercial use in handsets [19]. These antennas improve the handset efficiency by reducing the energy deposited in the users head, however, careful ergonomic design of the handset is needed or else absorption by the hand may become significant [18].

Due to their conformal nature and their robustness variants of the printed antenna can be used as small unobtrusive antennas. Unfortunately, printed antennas in their conventional form and at low-microwave frequencies take up too much antenna real estate. One approach to producing a smaller antenna is to incorporate a single shorting post located near the feed [20]. In our study, a rectangular shorted-patch antenna analogous to [20] is analyzed for application to mobile communications handsets. However, such patch antennas may not offer sufficient bandwidth for mobile communications systems. The bandwidth of a printed antenna can be in-

Manuscript received May 29, 1998; revised October 29, 1998.

J. T. Rowley is with Telstra Research Laboratories, Clayton, Victoria, 3168 Australia.

R. B. Waterhouse is with the Department of Communication and Electronic Engineering, Royal Melbourne Institute of Technology, Melbourne, Victoria, 3000 Australia.

Publisher Item Identifier S 0018-926X(99)04825-5.

[1] Remcom Inc., Calder Square, State College, PA 16805.

TABLE I
FDTD MESH TISSUE GROUPINGS AND CORRESPONDING TISSUES AVERAGED FROM THE WORK OF [15] TO PROVIDE THE DIELECTRIC PROPERTIES

FDTD Mesh Tissue	Gabriel tissues [15]	1800 MHz		
		ε_r	σ (S/m)	ρ (kg/m^3)
cartilage	cartilage	40.22	1.29	1000
muscle	muscle	53.55	1.34	1020
eye	sclera, cortex, nucleus, vitreous humour,	50.58	1.49	1000
nerve, brain	cerebellum, cerebro spinal fluid, white matter	50.11	1.85	1050
skin	skin (dry)	38.87	1.19	1000
fat, bone	averaged infiltrated fat and cortical bone	11.40	0.23	1200
blood	blood	59.37	2.04	1000

creased by parasitically coupling another printed radiator to the driven element in the vertical direction. This is known as stacking and importantly the surface area is not greatly increased. In this paper, we analyze the handset application of a novel probe-fed stacked shorted-patch, which displays enhanced bandwidth compared to a single-layer shorted patch [21]. Importantly, it also reduces the manufacturing tolerances on the relative position of the feed and shorting post.

Results are presented at 1800 MHz for each of the antennas: $\lambda/4$ monopole, shorted patch and stacked shorted patch, in each of three cases: on a handset in isolation, a handset near the realistic head model, and with the inclusion of a block model of the hand.

II. THE FDTD TECHNIQUE

The implementation of the FDTD technique used in the XFDTD code is described in detail by Kunz and Luebbers [22]. The COST244 [13] handset dimensions, 120 $\times$ 42.5 $\times$ 22.5 mm, are multiples of 2.5 mm so this was selected as the voxel size of the model which for stability leads to a time step of 4.12 ps. The antennas were excited with a gap voltage source specified with a 50-Ω series source impedance to simulate a real-voltage generator and reduce the number of time steps needed for convergence [23]. Transient excitation for 3500 time steps using a Gaussian derivative pulse was used to calculate the wide-band input impedance with a specified pulse width of 410 time steps (1.71 ns), which leads to a frequency spectrum that is more than 120 dB down at 2.2 GHz and reduces aliasing effects in the biological materials. Antenna patterns and SAR results were calculated using a steady-state sinusoidal excitation of 1800 MHz and were run for 4000 time steps (30 periods) to ensure converged results. Errors are increased in FDTD analyses if perfectly electric conductor (PEC) edges do not coincide with the Cartesian mesh. Therefore, the handset was held vertical in the mesh and a head model rotated forward and to the right so that the handset was in a realistic usage position relative to the head. The antenna patterns were "corrected" for the rotated head so that the patterns presented here represent the antenna on a handset in an actual usage position, i.e., with the head vertical and the handset inclined [16]. Second-order Liao outer radiation boundary conditions were used with a minimum 20–cell border established around the model.

III. HEAD MODEL WITH HANDSET IN A REALISTIC USAGE POSITION

A wide variety of computational phantoms have been used for SAR assessments of mobile communications type exposures ranging from homogeneous or layered spheres [13] to millimeter resolution anatomically realistic models [11]. A 3-mm voxel resolution head and shoulders mesh model was developed based on data from the Visible Human Project [14]. The mesh was resampled with 2.5-mm voxels and the shoulders were truncated to fit the available computer memory. The values of the tissue dielectric parameters at 1800 MHz were derived from recent work [15]. There are seven tissue groupings used in the head model. Where a one-to-one correspondance did not exist, the parameters for several tissue types from [15] were averaged before assignment to the FDTD mesh materials. The details of the tissue parameters are shown in Table I. The tissue densities are those provided with the mesh.

The CENELEC (European Committee for Electrotechnical Standardization) draft mobile telecommunications equipment (MTE) standard specifies the intended or normal operating position in terms of a reference plane and a reference line [16]. Fig. 1 shows this relationship and the orientation of the coordinate system. The reference plane is defined by the auditory canal openings and the centre of the closed mouth. The reference line is defined to be the "tangential" line that connects the center of the ear piece with the center bottom of the case. The phone is positioned so that the reference line lies in the reference plane and with the center of the ear piece in line with the entrance of the auditory canal. The handset is also positioned such that an angle of 80° exists between the reference line and the line connecting both auditory canal openings. To avoid staircasing effects on the handset the head model was rotated forward by 74° and to the right 10° to orientate the phone in the CENELEC intended position of

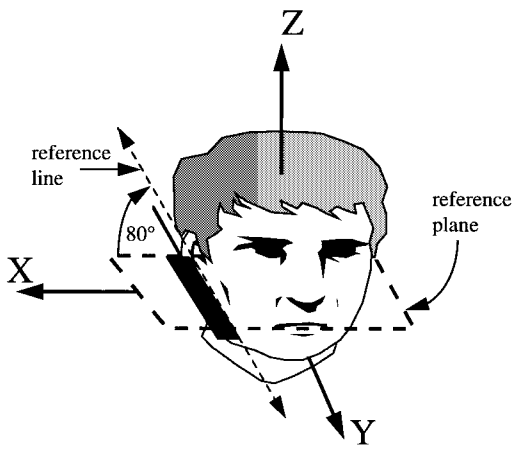

Fig. 1. Perspective view showing the effective orientation of the handset relative to the head and the coordinate system.

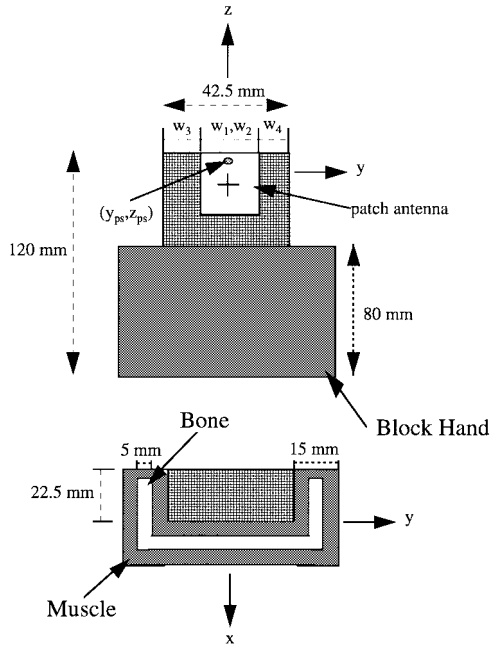

Fig. 2. View of the handset showing the location of the shorted-patch antenna and the dimensions of the block model hand.

use relative to the head. The handset was then placed on the right-hand side of the head model and aligned with the FDTD mesh.

The resampling of the head model for 2.5-mm voxels and the rotations were done on the original head mesh to minimize anatomical errors, however, any distortions are expected to be within the range of human variation. The major anatomical features were cross checked with an atlas of sectional anatomy before and after the resampling and rotation so that gross distortions would be detected [24]. The block model of the hand wraps around three sides of the lower half of the handset and consists of a core of bone surrounded with a layer of muscle similar to that used in [18]. Details of the hand model can be seen in Fig. 2. The resulting mesh has dimensions of $147 \times 161 \times 148$ ($\approx$3.4 million) cells requiring approximately 105 Mb of RAM. The analysis was run on a HP 715/100 with 128 Mbytes of RAM and took about 8 h for a transient or steady state excitation. The results for the antennas on the handsets in isolation used a space of $65 \times 70 \times 120$ cells and took just over 1 h to calculate.

TABLE II
DIMENSIONS OF THE SINGLE AND STACKED SHORTED PATCH ANTENNAS. REFER TO FIGS. 2 AND 3 FOR DETAILS

	Single Patch	Stacked Patch
$L_1 = L_2$	17.5 mm	17.5 mm
$W_1 = W_2$	25 mm	15 mm
W_3	10 mm	7.5 mm
W_4	15 mm	12.5 mm
d_1	10 mm	5.0 mm
d_2	N/A	7.5 mm
(y_p , z_p)	(0 , 1.25) mm	(0 , 1.25) mm
(y_{ps} , z_{ps})	(0 , 3.75) mm	(0 , 6.25) mm
$r_0 = r_{0s}$	0.6 mm	0.6 mm
e_{r1}, s_1	1.07, $1\text{x}10^{-4}$ S/m	1.07, $1\text{x}10^{-4}$ S/m
e_{r2}, s_2	N/A	2.2, $1\text{x}10^{-4}$ S/m

IV. MONOPOLE AND SHORTED PATCH ANTENNA MODELS

The COST244 monopole is specified to be $\lambda/4$ with a diameter of 2.5 mm and a feed gap of 2.5 mm. The antenna is positioned in the center top of the handset and is modeled as a column of perfectly conducting cells as it has been reported that for the present cell size and the specified antenna diameter the column approach yields the most accurate simulations [25]. At 1800 MHz, $\lambda/4$ corresponds to an overall antenna length of 16.7 cells, which is rounded down to 15 cells plus gap. The distance between the feed point and the head is specified as 1.5 cm. The gap-voltage source feeds the monopole on a corner, which results in some asymmetry in the calculated antenna patterns.

Printed antennas have found limited use in applications such as mobile communication handset terminals [19]. In large measure this may be because in their conventional form at present mobile communications frequencies printed antennas occupy a lot of handset area. There are several new configurations that successfully reduce the physical size of a printed antenna. One of the simplest approaches is to incorporate high-dielectric constant substrates and cover layers [26]. However, this technique results in very narrow bandwidths and stringent manufacturing tolerances and is therefore unsuitable for many applications. Several versions of a shorted patch have also been proposed [20], [27], [28]. It is a variation on [20] modified to suit the rectangular FDTD grid, which forms the single shorted-patch antenna. A common technique to enhance the bandwidth of a printed antenna is to parasitically couple another radiator to the driven element and a version with a coplanar parasitic element was presented in [27], using a shorted patch and an annular ring. Although this antenna had a bandwidth greater than 10%, the increase in surface area may not be acceptable in some applications. We have developed a rectangular probe-fed stacked shorted patch [21] with increased bandwidth and reduced surface area, which we here investigate for handset applications.

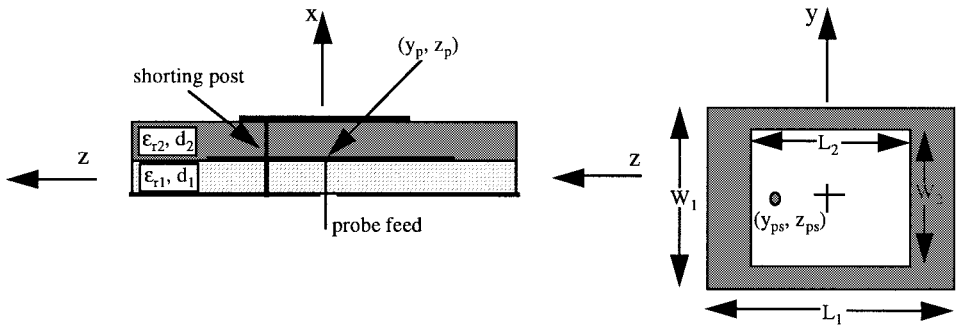

Fig. 3. Schematic of a stacked shorted probe-fed rectangular microstrip patch antenna.

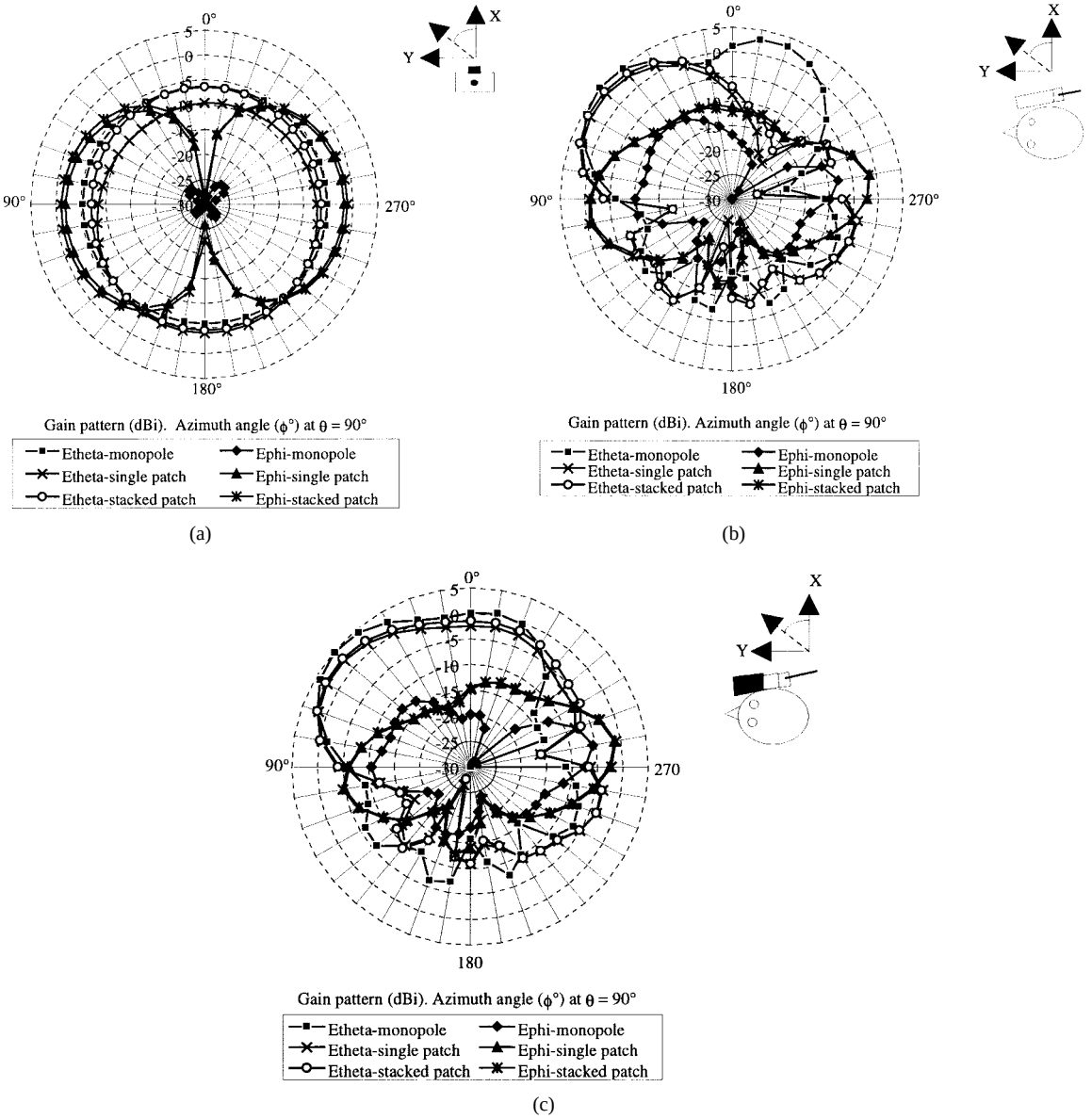

Fig. 4. Azimuth ($\theta = 90°$) gain patterns computed using the FDTD method for the monopole, single, and stacked patches on: (a) the vertical handset in isolation; (b) the handset adjacent to the head rotated to the CENELEC normal position of use; and (c) including the block model hand.

Fig. 3 shows a schematic of a stacked probe-fed rectangular shorted patch. The single shorted patch takes the same shape but only has a single dielectric layer and radiating patch. In the general case of the stacked patch, the driven patch of length L_1 and width W_2 can be etched on a substrate of thickness d_1 and with a dielectric constant ε_{r1}. The driven patch is fed by a coaxial probe of radius r_0 located at (y_p, z_p) from the center of the patch. The shorting post of radius r_{0s} positioned at

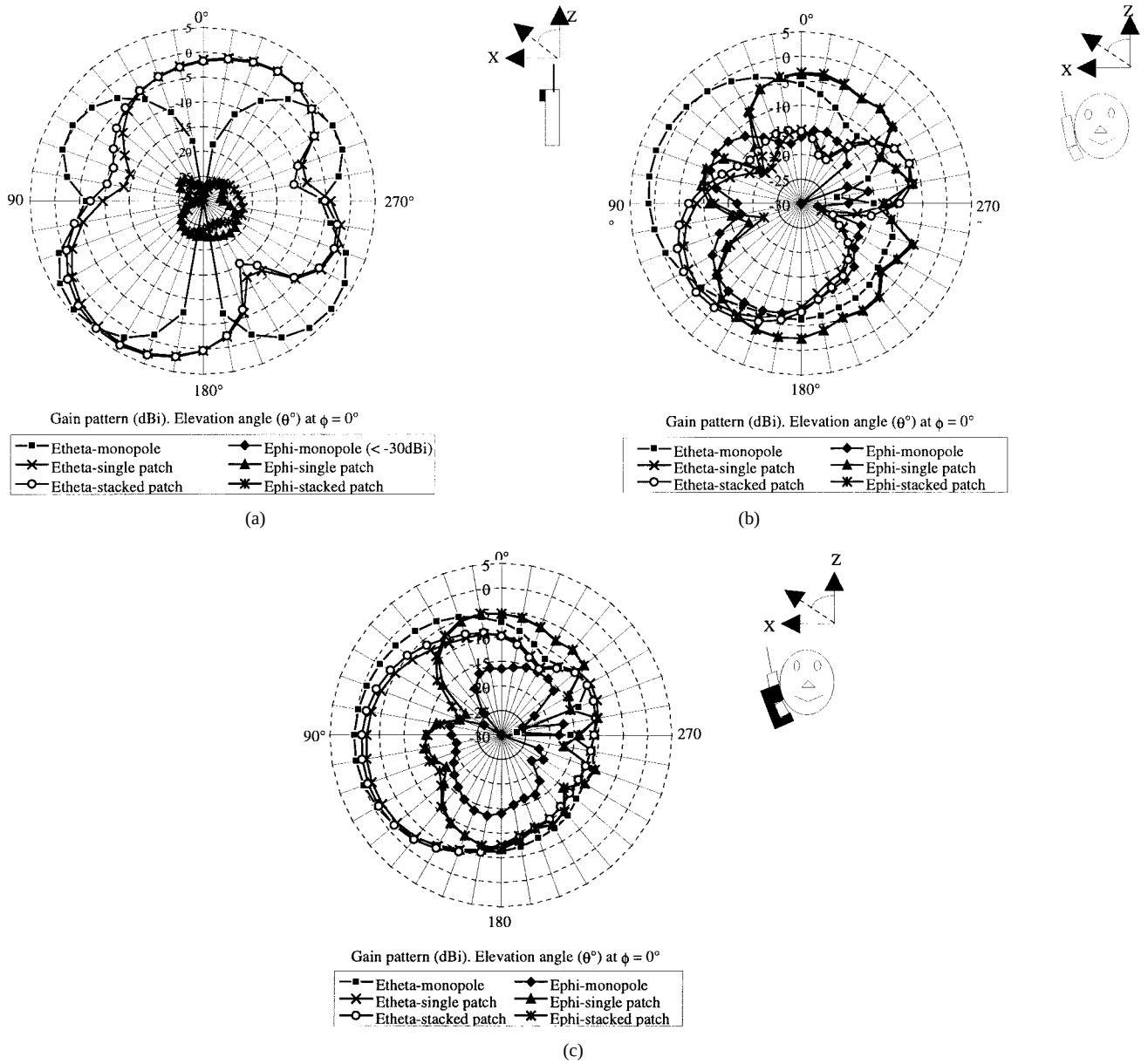

Fig. 5. Elevation ($\phi = 0^\circ$) gain patterns computed using the FDTD method for the monopole, single, and stacked patches on: (a) the vertical handset in isolation; (b) the handset adjacent to the head rotated to the CENELEC normal position of use; and (c) including the block model hand.

(y_{ps}, z_{ps}) is connected to and extends through the first printed conductor and is soldered to the second patch of dimensions L_2 and W_2. For the stacked-patch antenna, a dielectric layer of height d_2 and dielectric constant ε_{r2} separates the two patch conductors. In this study, the patch antennas are mounted on the back of the handset in line with the upper edge (see Fig. 2 for location details). The dimensions for each of the patch antennas are listed in Table II.

V. Comparison of Antenna Performance

In this section, the computed principal E- and H-plane antenna patterns as well as $|S_{11}|$ are presented for each of the antennas on a handset in isolation, near the rotated realistic head model and with the addition of a block model hand. In order to get a clearer picture of these antennas during use, the antenna patterns with the head present are "corrected" for the rotation of the head so that they represent the antenna patterns with the handset in the intended position of use. The antenna radiation patterns for the antennas on the handset in isolation are not transformed as it was observed that handsets are generally positioned in an upright orientation when not in use.

The azimuth patterns computed using the FDTD methods of Section II for the antennas on the handset in isolation are shown in Fig. 4(a). We see that the monopole has an essentially omnidirectional pattern; the reason for the slight deviation is the noncentral excitation of the antenna. The two shorted-patch antennas exhibit similar patterns with about a 5-dB front-to-back ratio (F/B) for the single patch and 2.5 dB for the stacked patch. When the head and hand are introduced the patterns [Fig. 4(b), (c)] become much more complicated with many smaller lobes; however, on average, each of the antennas offers similar performance.

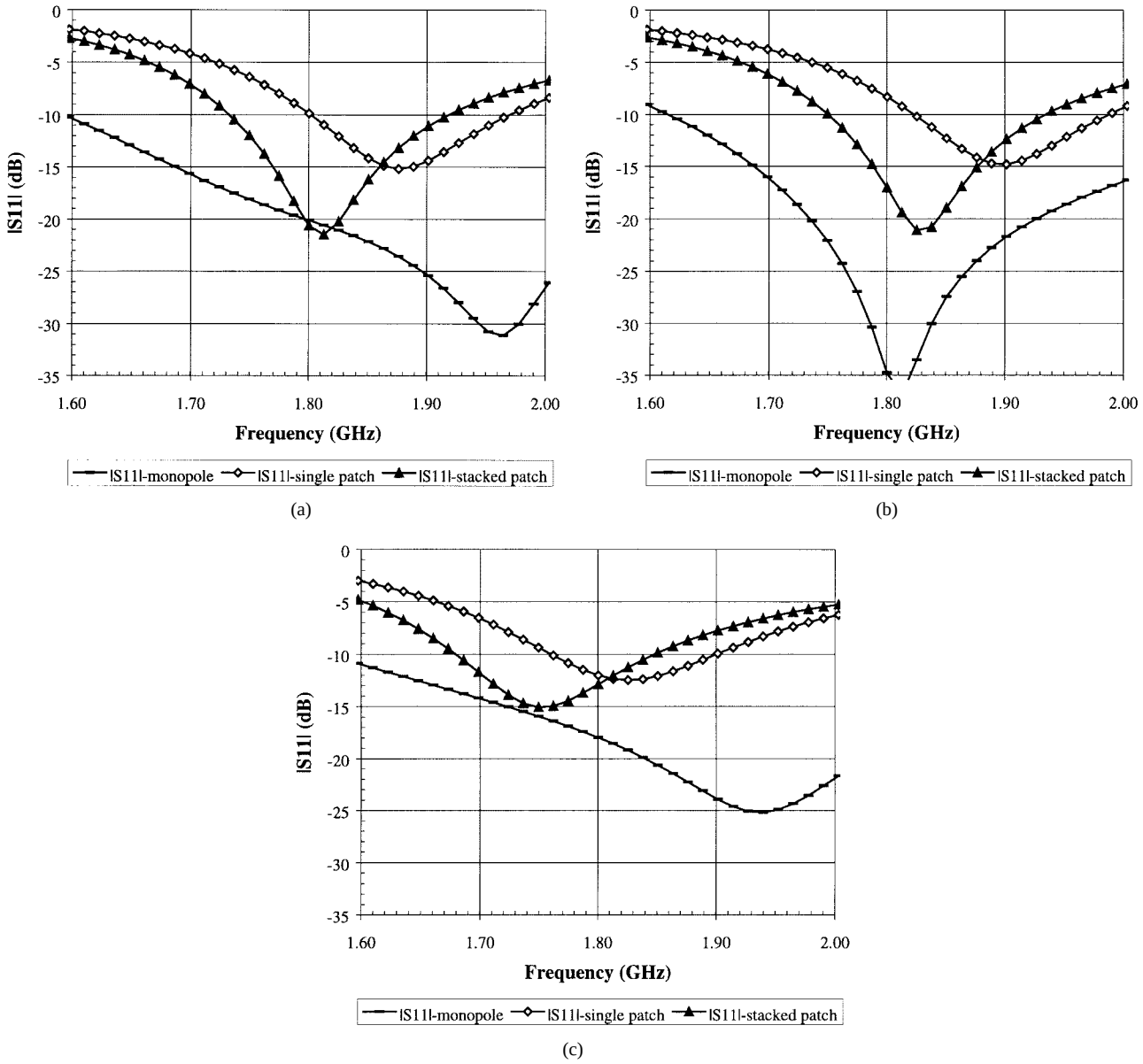

Fig. 6. $|S_{11}|$ versus frequency computed using the FDTD method for the monopole, single and stacked patches on: (a) the vertical handset in isolation; (b) the handset adjacent to the head rotated to the CENELEC normal position of use; and (c) including the block model hand.

The elevation patterns for the monopole on the handset shown in Fig. 5(a) are downtilted (peak gain of 4.12 dBi at $\theta = 130°$) and have a split main lobe, which typically occurs on handsets that are long relative to the wavelength [29]. Microstrip antennas on infinite ground planes exhibit almost complete coverage over 180° in the broadside direction. Mounting adjacent to the upper edge of the handset leads to diffraction of the fields over the top edge of the handset and splitting of the main beam with a downtilted lobe (single patch peak gain 3.24 dBi at $\theta = 150°$, stacked-patch peak gain 3.64 dBi at $\theta = 150°$) similar to the monopole. The patch antenna patterns peak approximately 4 dB lower than the monopole in the front (side toward the operators face: $\phi = 180°$) of the handset which implies less RF current flow on this surface. The introduction of the rotated head manifests itself in the patterns of Fig. 5 (b) and (c) as a general reduction in level in the half-space occupied by the head and the raising of the cross-polar components. The monopole main lobe is quite broad and peaks at 1.45 dBi at the angle $\theta = 70°$ so that it is orientated close to the horizon with the handset in the normal position of use. The main lobe of the patch antenna patterns is directed to $\theta = 130°$, which is somewhat below the horizon, but this may not be significant in a multipath environment. There is also a secondary peak at about $\theta = 290°$ due to diffraction over the top edge of the handset and around the head. There is remarkable similarity between the copolar elevation patterns of the three antenna types when the hand is introduced. The presence of the hand tends to reduce the variation of the patterns due to absorption of the RF currents flowing on the handset.

The $|S_{11}|$ plots for each of the antennas in Fig. 6 provide further insight into the interaction of the RF current flows on the handset with the head and hand. The monopole shows the widest -10-dB bandwidth of the three antennas in all

TABLE III
COMPARISON OF MAXIMUM 1-g SAR VALUES IN THE HEAD, NORMALIZED TO 1 W OF INPUT POWER, AND EFFICIENCY FOR EACH OF THE ANTENNAS WITH AND WITHOUT THE BLOCK MODEL HAND

	No Hand		With Hand	
	1 g SAR	η	1 g SAR	η
Monopole	4.80 W/kg	60.3 %	3.92 W/kg	50.5 %
Single patch	1.50 W/kg	79.0 %	1.00 W/kg	69.0 %
Stacked patch	1.53 W/kg	79.6 %	0.92 W/kg	69.3 %

three situations. In Fig. 6(a) for the handset in isolation the monopole shows a −10-dB bandwidth of 35.5%, the single patch 10%, and the stacked patch 11.7%. The single patch is not centered on the nominal frequency of 1.8 GHz due to the limitations of the 2.5-mm grid. A more refined grid would allow the patch length to be slightly increased to improve the match, but the present model is sufficient to illustrate the relative trends. It should be noted that the larger bandwidth of the stacked-patch configuration was achieved in 60% of the patch area and 75% of the volume occupied by the single-layered version. Larger bandwidths could have been achieved using thicker material, however, a compromise with respect to ergonomic considerations would need to be made. When the head is included, the two patch antennas show [Fig. 6(b)] an upward shift in the frequency of the VSWR minimum while the monopole shifts downwards. The −10-dB bandwidths are now 32.2% for the monopole, 10% for the single patch and 10.5% for the stacked patch. The block hand causes an overall reduction in the degree of the match for all the antennas. The three antenna types show [Fig. 6(c)] a downward shift in the position of the maximum return loss relative to the situation of the handset in isolation so that all the antennas are matched at 1800 MHz. The bandwidths are 37.8% for the monopole, 8.2% for the single patch, and 9.4% for the stacked patch.

Table III and Fig. 7(a)–(f) compares the SAR distributions for each of the antenna types. A previous study which modeled a $\lambda/4$ monopole at 1900 MHz close to an upright or $\theta = 30°$ forward tilted head found peak 1-g SAR's of 8.88 and 8.64 W/kg, respectively, for 1 W of time averaged radiated power [11]. The lower SAR's in our study are explained by the finite return loss of the antennas and the rotation of the head placing the antenna further from the surface of the head. The peak spatial SAR's for the shorted-patch antennas are about one third of those for the monopole. This is better than the reduction seen at 900 MHz with planar inverted-F antennas mounted on the back of a handset [18] and can be attributed to the better directivity achievable at higher frequencies. For each of the antennas the inclusion of the hand in the present position reduces the efficiency η by about 10%; from 60.3% to 50.5% for the monopole and from approximately 79% to 69% for the patch antennas. However, if the hand is moved further up, the handset the efficiencies of the shorted-patch antennas is expected to degrade faster than that of the monopole due to current flows and possible physical obstruction of the antenna [18]. The SAR contours of Fig. 7(a)–(f) show the monopole to be exposing a wide area of the side of the head, whereas the shorted-patch antennas show distinct volumes of absorption in the area of the ear and the cheek. The shorted-patch antennas produce higher SAR's in the hand than does the monopole due to the greater current flows on the handset case.

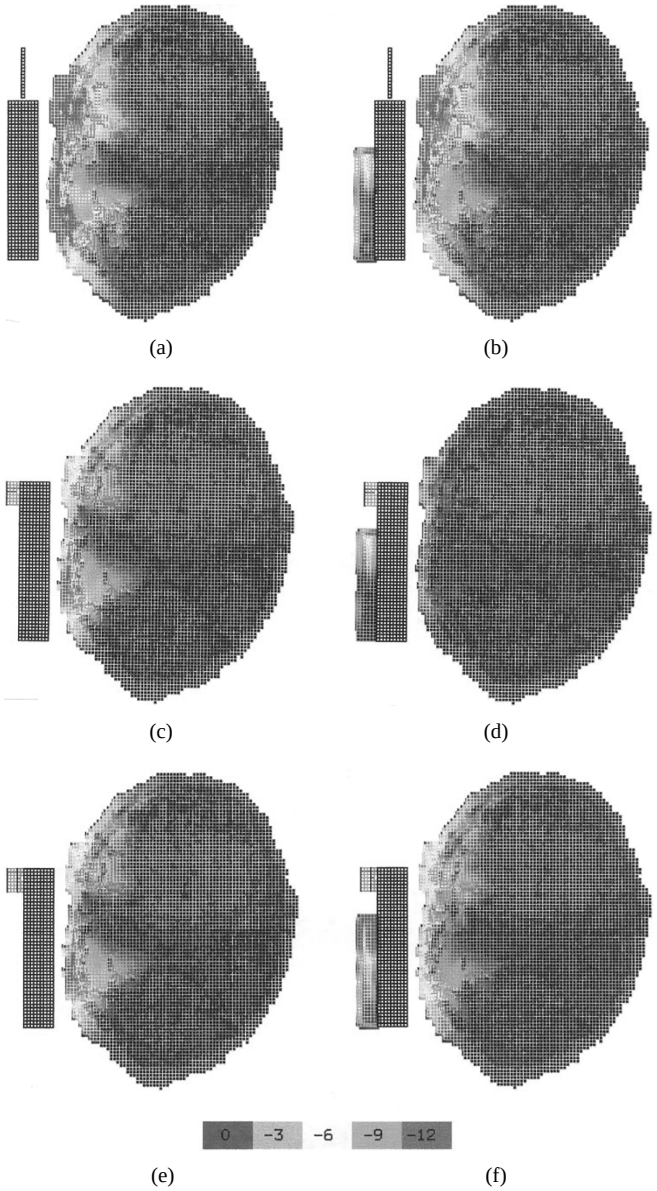

Fig. 7. (a)–(f) Unaveraged SAR contours normalized to 1.6 W/kg for 1 W of input power for each antenna adjacent to the realistic head model rotated to the CENELEC intended position of use with and without block model hand.

VI. DISCUSSION AND CONCLUSIONS

Results have been presented for a monopole and two types of shorted-patch antennas at 1800 MHz on an isolated handset in the presence of a head with and without a block model hand. The anatomically detailed head model has been rotated to correspond to the CENELEC intended position of use to obtain a comparison of antenna performances in a position of actual handset use. The move to higher frequencies for mobile communications services will allow the possible use of more sophisticated directional antenna types on mobile communications handsets. However, it has also been reported that for some environments an omnidirectional pattern reduces the probability of poor call quality performance, but as the

number of indirect paths increases this advantage vanishes [30]. As the higher frequency services are likely to be used in built up areas involving complex multipath propagation paths shorted-patch antennas could be used on handsets. The selection of a single- or stacked-element shorted-patch antenna would largely be determined by the available handset antenna real estate and/or the required bandwidth. These antennas offer better efficiencies than monopole antennas at 1800 MHz through directing more of the phone's radio transmissions away from the users head so that peak spatial 1-g SAR's are reduced by approximately 70%. Ergonomic design of the handset is needed to ensure that the user is discouraged from placing a hand over the antenna element.

REFERENCES

[1] International Commission Non-Ionizing Radiation Protection, "Health issues related to the use of hand-held radiotelephones and base transmitters," *Health Phys.*, vol. 70, no. 4, pp. 587–593, Apr. 1996.

[2] A. McKinlay, "Radiotelephones and human health: A European research initiative," *Radiation Protection Dosimetry*, vol. 72, no. 3–4, pp. 313–320, 1997.

[3] N. Kuster and Q. Balzano, "Energy absorption mechanism by biological bodies in the near field of dipole antennas above 300 MHz," *IEEE Trans. Veh. Technol.*, vol. 41, pp. 17–23, Feb. 1992.

[4] Q. Balzano, O. Garay, and T. J. Manning, Jr., "Electromagnetic energy exposure of simulated users of portable cellular phones," *IEEE Trans. Veh. Technol.*, vol. 44, pp. 390–403, Aug. 1995.

[5] ANSI/IEEE C95.1-1992, *American National Standard—Safety Levels with Respect to Exposure to Radio Frequency Electromagnetic Fields, 3 kHz–300 GHz*. New York: IEEE Press, 1992.

[6] Federal Communications Commission—Guidelines for Evaluating the Environmental Effects of Radiofrequency Radiation, FCC 96-326, Aug. 1, 1996.

[7] N. Kuster, R. Kästle, and T. Schmid, "Dosimetric evaluation of handheld mobile communications equipment with known precision," *IEICE Trans. Communicat.*, vol. E80-B, no. 5, pp. 645–652, May 1997.

[8] M. Hussein and A. Sebak, "Application of the finite-difference time-domain method to the analysis of mobile antennas," *IEEE Trans. Veh. Technol.*, vol. 45, pp. 417–426, Aug. 1996.

[9] M. Okoniewski and M. A. Stuchly, "A study of the handset antenna and human body interaction," *IEEE Trans. Microwave Theory Tech.*, vol. 44, pp. 1855–1864, Oct. 1996.

[10] M. Taki, S. Watanabe, and T. Nojima, " FDTD analysis of electromagnetic interaction between portable telephone and human head," *IEICE Trans. Electron.*, vol. E79-C, no. 10, pp. 1300–1307, Oct. 1996.

[11] O. P. Gandhi, G. Lazzi, and C. M. Furse, "Electromagnetic absorption in the human head and neck for mobile telephones at 835 and 1900 MHz," *IEEE Trans. Microwave Theory Tech.*, vol. 44, pp. 1884–1897, Oct. 1996.

[12] XFDTD, *User's Manual for XFDTD the X-Window Finite Difference Time Domain Graphical User Interface for Electromagnetic Calculations*, version 4.03, Remcom Inc., June 1997.

[13] G. D'Inzeo, "Proposal for numerical canonical models in mobile communications" in *Biomedical Effects of Electromagnetic Fields—Reference Models in Mobile Communications*, D. Šimunić, Ed. Rome, Italy: COST244, 1994, pp. 1–7.

[14] R. Luebbers, "FDTD predictions of electromagnetic fields in and near human bodies using visible human project anatomical scans," in *Proc. Antennas Propagat. Soc. Annu. Symp.*, Baltimore, MD, 1996, vol. 3, pp. 1806–1809.

[15] C. Gabriel, "Compilation of the dielectric properties of body tissues at RF and microwave frequencies," Brooks Air Force Base, TX, Rep. AL/OE-TR-1996-0037, 1996.

[16] SC211B of CENELEC TC 211, *Considerations for Evaluation of Human Exposure to Electromagnetic Fields (EMF's) From Mobile Telecommunication Equipment (MTE) in the Frequency Range 30 MHz–6 GHz*. Brussels, Belgium: CENELEC, 1997.

[17] G. F. Pederson and J. B. Anderson, "Integrated antennas for hand-held telephones with low absorption," in *IEEE Veh. Technol. Conf.*, Stockholm, Sweden, June 1994, pp. 1537–1541.

[18] M. A. Jensen and Y. Rahmat-Samii, "EM interaction of handset antennas and a human in personal communications," *Proc. IEEE*, vol. 83, pp. 7–17, Jan. 1995.

[19] G. A. Kyriacou and J. N. Sahalos, "Analysis of a probe-fed short-circuited microstrip antenna," *IEEE Trans. Veh. Technol.*, vol. 45, pp. 427–430, Aug. 1996.

[20] R. B. Waterhouse, "Small microstrip patch antenna," *Electron. Lett.*, vol. 31, no. 8, pp. 604–605, Apr. 13, 1995.

[21] R. B. Waterhouse, J. T. Rowley, and K. H. Joyner, "Stacked shorted patch antenna," *Electron. Lett.*, vol. 34, no. 7, pp. 612–614, Apr. 2, 1998.

[22] K. S. Kunz and J. Luebbers, *The Finite Difference Time Domain Method for Electromagnetics*. Orlando, FL: CRC, 1993.

[23] R. Luebbers and H. S. Langdon, "A simple feed model that reduces time steps needed for FDTD antenna and microstrip calculations," *IEEE Trans. Antennas Propagat.*, vol. 44, pp. 1000–1005, July 1996.

[24] W. J. Bo, N. T. Wolfman, W. A. Krueger, and I. Meschan, *Basic Atlas of Sectional Anatomy with Correlated Imaging*, 2nd ed. Sydney, Australia: Saunders, 1990.

[25] I. G. Marqvardsen, "Numerical solution to the COST 244 problems using FDTD," *Biomedical Effects of Electromagnetic Fields—Reference Models in Mobile Communications*, D. Šimunić, Ed. Rome, Italy: COST244, Nov. 1994, pp. 55–66.

[26] T. K. Lo, C.-O. Ho, Y. Hwanf, E. K. W. Lam, and B. Lee, "Miniature aperture-coupled microstrip antenna of very high permittivity," *Electron. Lett.*, vol. 33, pp. 9–10, Jan. 1997.

[27] R. B. Waterhouse, "Printed antenna suitable for mobile communication handsets," *Electron. Lett.*, vol. 33, pp. 1831–1832, Oct. 1997.

[28] I. Park and R. Mittra, "Aperture-coupled small microstrip antenna," *Electron. Lett.*, vol. 32, pp. 1741–1742, Sept. 1996.

[29] R. Yamaguchi, K. Sawaya, Y. Fujino, and S. Adachi, "Effect of dimension of conducting box on radiation pattern of a monopole antenna for portable telephone," *IEICE Trans. Commun.*, vol. E76-B, no. 12, pp. 1526–1531, Dec. 1993.

[30] I. Shtrikman, H. Lindenborn, and H. Fruechting, "Performance and electromagnetic compatibility analysis of antennas for hand held mobile telephones," *26th Eur. Microwave Conf.*, Prague, Czech Republic, Sept. 1996, vol. 1, pp. 246–250.

Jack T. Rowley (M'98) was born in London, U.K., in 1967. He received the B.Eng. degree (honors) in electronic engineering from the University of Limerick, Ireland, in 1989. He is currently working toward the Ph.D. degree at the Royal Melbourne Institute of Technology University (RMIT), Melbourne, Australia.

In 1989, he joined the Mobile Communications Division of Telstra, Australia, and in 1990 moved to the Electromagnetic Compatibility Section of the Telstra Research Laboratories where he was involved in the test and measurement of antennas and the development of computational models. In 1993 he joined the Radio Frequency Safety and Interference Research Program, Telstra Research Laboratories and in 1998 became the leader of that group. His research interests are in the application of computational electromagnetics and radio frequency dosimetry to investigate possible health and interference effects of radio services and in the development of occupational safety policies.

Rod B. Waterhouse (S'90–M'93), for a photograph and biography, see p. 388 of the February 1999 issue of this TRANSACTIONS.